Selective Excitation of Terahertz Magnetic and Electric Dipoles in Er^{3+} Ions by Femtosecond Laser Pulses in $ErFeO_3$

R. V. Mikhaylovskiy,[1,*] T. J. Huisman,[1] R. V. Pisarev,[2] Th. Rasing,[1] and A. V. Kimel[1]

[1]*Radboud University, Institute for Molecules and Materials, Heyendaalseweg 135, 6525 AJ Nijmegen, Netherlands*
[2]*Ioffe Physical-Technical Institute, Russian Academy of Sciences, 194021 St. Petersburg, Russia*

We show that femtosecond laser pulse excitation of the orthoferrite $ErFeO_3$ triggers pico- and subpicosecond dynamics of magnetic and electric dipoles associated with the *low energy* electronic states of the Er^{3+} ions. These dynamics are readily revealed by using polarization sensitive terahertz emission spectroscopy. It is shown that by changing the polarization of the femtosecond laser pulse one can excite either electric dipole-active or magnetic dipole-active transitions between the Kramers doublets of the $^4I_{15/2}$ ground state of the Er^{3+} ($4f^{11}$) ions. These observations serve as a proof of principle of polarization-selective control of both electric and magnetic degrees of freedom at terahertz frequencies, opening up new vistas for optical manipulation of magnetoelectric materials.

The coupling of femtosecond laser pulses to magnetic excitations is a heavily debated topic in several areas of contemporary physics, including ultrafast magnetism [1], multiferroics [2,3], spintronics [4–6], and magnonics [7,8]. The results of this fundamental research may have tremendous impact on information storage technologies. Impulsive stimulated Raman scattering (ISRS) offers a proven way to excite magnetic resonances in media by light at the subpicosecond time scale [1]. By choosing the polarization of light or propagation direction, it is possible to attain a selective excitation of a particular resonance mode [9,10]. To date, such a selective excitation of magnetization dynamics was demonstrated only for magnetic dipole-active modes. In this Letter, we show that ISRS can selectively excite not only magnetic dipoles, but also electric dipole-active magnetic resonances, greatly extending the potential for optically encoding information in solids.

To this end, we have conducted terahertz (THz) emission spectroscopy measurements on single crystals of erbium orthoferrite $ErFeO_3$. Er^{3+} ions in $ErFeO_3$ have magnetic and electric-dipole active transitions which have slightly different frequencies lying in the THz range. The magnetic and electric-dipole transitions must be excited by laser pulses with different polarizations as they have different selection rules. Despite extensive investigations of the laser-induced spin dynamics in rare-earth orthoferrites [11–17], to date the laser excitation of the electronic transitions in the rare-earth ions has been mostly ignored.

$ErFeO_3$ has a distorted perovskite crystal structure with D_{2h}^{16} space group. Its unit cell contains four magnetic Fe^{3+} ions forming two antiferromagnetically ordered sublattices with a small canting due to the presence of the Dzyaloshinskii-Moriya interaction. The Néel temperature for the iron sublattices is $T_N^{iron} \approx 650$ K. Below $T_1 = 80$ K the magnetic phase has Γ_2 symmetry with the iron spins

oriented along the crystallographic z axis with a canting towards the x axis [see Fig. 1(a)]. Above $T_2 = 95$ K the magnetic phase has the Γ_4 symmetry with the iron spins oriented along the x axis with a canting towards the z axis [see Fig. 1(b)]. In the temperature interval between T_1 and T_2 the erbium orthoferrite exhibits a spin reorientation when the iron spins continuously rotate in the (xz) plane. The Er^{3+} ions are in a paramagnetic state above their Néel temperature $T_N^{erbium} \approx 4$ K, being polarized by the exchange interaction with the iron sublattices and forming a canted configuration in the (xz) and (yz) planes in the Γ_2 and Γ_4 magnetic phases, respectively [18]. The net magnetic moment of the Er^{3+} ions is always oriented antiparallel with respect to the weak magnetic moment of the Fe^{3+} sublattices and rotates by 90° together with the spin reorientation of the latter (see Fig. 1) [19].
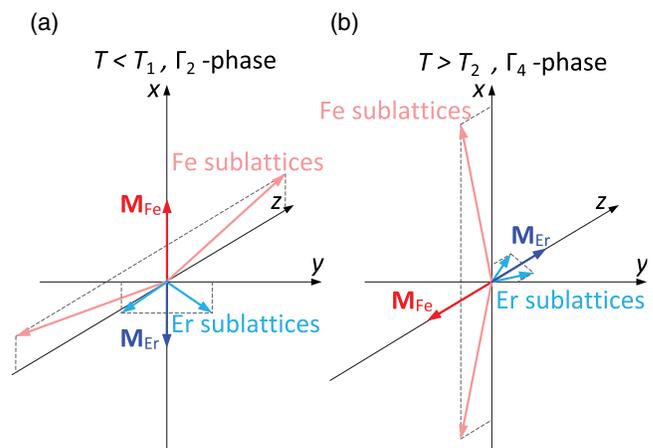

FIG. 1. Arrangement of magnetic moments of the Fe^{3+} and Er^{3+} sublattices of $ErFeO_3$ in the Γ_2 (a) and Γ_4 phases (b).
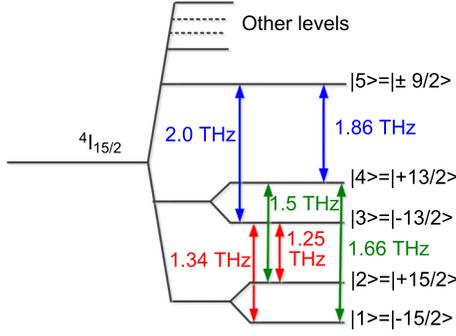
FIG. 2.   The energy level structure of the ground state $^4I_{15/2}$ of the Er^{3+} ion in $ErFeO_3$ [18] and the possible transitions marked by arrows.

The rare-earth Er^{3+} ions occupy off-centrosymmetric sites with C_s local symmetry thus allowing electric-dipole active transitions of their electrons within the $4f$ shell [20]. However, the presence of a macroscopic electric polarization at equilibrium is prohibited by symmetry [21]. The low local symmetry of the rare-earth sites leads to the complete splitting of the ground state $^4I_{15/2}$ of the Er^{3+} ions into eight doublets with Kramers-conjugated states [18]. The Er-Fe exchange leads to the breaking of the time-reversal symmetry and, consequently, splitting of the Kramers doublets. The energy-level structure of the ground multiplet of the Er^{3+} ion in the orthoferrite is schematically shown in Fig. 2. The symmetry of the macroscopic normal modes arising from the transitions in Er^{3+} ions is determined by the irreducible representations of the space group D_{2h}^{16} and they are summarized in Table I [20,22–24]. The transitions between the states belonging to the different doublets are fourfold degenerate consisting of two electric dipole and two magnetic dipole modes of different symmetry in the Γ_4 and Γ_2 phases. During the spin reorientation from the Γ_2 to the Γ_4 phase the polarization of the rare-earth modes changes, following the rotation of the corresponding dipole components in the (xz) plane. We note that the modes with

different symmetry corresponding to the same transition have slightly different frequencies [20].

To study the optical excitation of low-energy electronic transitions in Er^{3+} ions we employed the THz emission spectroscopy setup described in Ref. [25]. We studied $ErFeO_3$ single crystal plates cut perpendicularly to the y and x crystallographic axes, respectively. The samples were excited by 40 fs laser pulses with their photon energy centered at 1.55 eV (wavelength 800 nm). The terahertz radiation generated in the sample was collected and refocused by a pair of off-axis parabolic mirrors onto a 1 mm thick electro-optic ZnTe crystal. The crystal was gated by the femtosecond pulses split from the pump beam. As the gating pulse copropagates with the THz wave it acquires ellipticity proportional to the terahertz electric field. By measuring this ellipticity and varying the time delay between the pump and the gate we are able to record the time evolution of the emitted terahertz waveform [26]. To measure orthogonal polarizations of the THz emission the samples were rotated around their normal with respect to the axis of the detecting ZnTe crystal. The geometry of the experiments for the y-cut and x-cut samples is schematically drawn in Figs. 3(a) and 3(b), respectively. Note that our experimental method allows detection of the THz emission polarized in the (xz) plane and (yz) plane for the y-cut and x-cut sample, respectively. The expected polarization of the emitted electric field for the different Er modes in these two cases is shown in the two last columns of Table I. The strong point of the THz technique is its sensitivity to both electric and magnetic dipole active modes.

The ISRS-based excitation of magnetic resonances is described, invoking the effective field model [9]. The magnetic dipole-active modes can be excited by an effective magnetic field $\mathbf{B}_{eff} = -\partial W/\partial \mathbf{M}$, where W is the free energy and $\mathbf{M}$ is the magnetization. One may anticipate that the magnetic dipole-active modes of Er^{3+} ions will be excited via processes phenomenologically described using

TABLE I.   Eigenmodes of the Kramers rare-earth ions in the orthoferrites. The oscillating components of the terahertz magnetic dipole moment $\mathbf{m}$ and the electric dipole moment $\mathbf{d}$ are indicated with respect to the crystallographic x, y, and z axes. The corresponding polarization of the emitted electric field is shown for the crystal plates cut perpendicularly to the y and x axes.

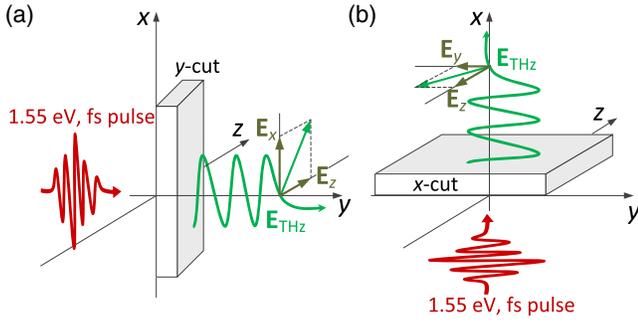| Magnetic phase	Mode symmetry (representation of group $D_{2h}{}^{16}$)	Transition between doublets			THz emission polarization	
		Magnetic dipole	Electric dipole	Degeneracy	y-cut	x-cut
Γ_4	Γ^+_{14}	m_z	$\cdots$	4	E_x	E_y
	Γ^+_{23}	m_x, m_y	$\cdots$	4	E_z	E_z
	Γ^-_{58}	$\cdots$	d_z	4	E_z	E_z
	Γ^-_{67}	$\cdots$	d_x, d_y	4	E_x	E_y
Γ_2	Γ^+_{12}	m_x	$\cdots$	4	E_z	$\cdots$
	Γ^+_{34}	m_y, m_z	$\cdots$	4	E_x	E_y, E_z
	Γ^-_{56}	$\cdots$	d_x	4	E_x	$\cdots$
	Γ^-_{78}	$\cdots$	d_y, d_z	4	E_z	E_y, E_z

FIG. 3.   The geometry of the optical pump/THz emission experiment. The direction of the laser pulse propagation and of the THz emission; the measured polarization of the THz electric field are shown with respect to the crystallographic axes. (a) The y-cut sample emits electric field polarized in the (xz) plane. (b) The x-cut sample emits electric field polarized in the (yz) plane.

an effective magnetic field $\mathbf{B}_{\text{eff}} = \hat{\chi}^{(m)} \mathbf{E}_{\text{opt}} \mathbf{E}_{\text{opt}}^*$, where $\mathbf{E}_{\text{opt}}$ is the complex envelope of the optical electric field and $\hat{\chi}^{(m)}$ is a phenomenological tensor describing ISRS involving virtual electric dipole transitions at the pump optical wavelength. In the simplest case of an isotropic medium the effective magnetic field $\mathbf{B}_{\text{eff}} \sim \lfloor \mathbf{E}_{\text{opt}} \times \mathbf{E}_{\text{opt}}^* \rfloor$ is generated by circularly polarized light.

To excite electric dipole-active modes one must act on the electronic system with an effective electric field $\mathbf{E}_{\text{eff}}$. In centrosymmetric crystals, such as $ErFeO_3$, the generation of the effective electric field via electric dipole-active optical transitions is forbidden. The lowest order process for generating such a field reads phenomenologically as $\mathbf{E}_{\text{eff}} = \hat{\chi}^{(e)} \mathbf{E}_{\text{opt}} \mathbf{H}_{\text{opt}}^*$, where $\mathbf{H}_{\text{opt}}$ is the complex envelope of the optical magnetic field and $\hat{\chi}^{(e)}$ is a tensor describing ISRS involving virtual magnetic dipole transitions at optical wavelengths. For photon energies around 1.55 eV, several f-f magnetic dipole optical transitions in Er^{3+} ions are clearly seen in the absorption spectrum of $ErFeO_3$ [27].

Indicative THz waveforms generated at $T = 20$ K by circularly polarized laser pulses of opposite helicities in the y-cut $ErFeO_3$ sample are shown in Fig. 4(a). The complex
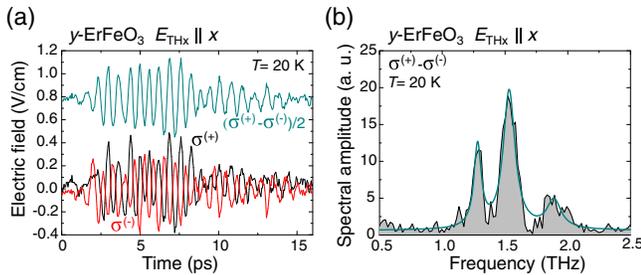

FIG. 4.   (a) The THz waveforms generated in the y-cut $ErFeO_3$ at 20 K by circularly polarized light of opposite helicities. The half-difference of these waveforms is shown shifted along the vertical axis. (b) The spectrum of the helicity dependent contribution obtained by Fourier transformation of the waveform shown in (a) and fitted with three Lorentzian contours.

emission spectrum consists of several narrow bands. Some of them with frequencies below 1 THz correspond to the magnetic resonances of the Fe^{3+} sublattices as it was reported earlier [25,28]. Here we focus on the spectral components lying above 1 THz [Fig. 4(b)].

We found that the spectral components lying above 1 THz are observed below ~150 K. Some of them are excited by the circularly polarized pump pulses with their initial phase determined by the pump helicity, while others were found to be sensitive neither to the circular nor to the linear polarization of the pump. The emitted THz waves have an electric field polarized along the x and z axes in the y-cut sample, but only along the y axis in the x-cut sample. Figures 5(a), 5(b), and 5(c) summarize the frequencies of all spectral components lying above 1 THz as a function of temperature [29].

As one can see from Fig. 5, the spectrum of THz emission above 1 THz consists of several components with frequencies lying at ~1.3, ~1.5, and ~1.8 THz. These values are close to the expected transitions between states belonging to the three lowest doublets of the Er^{3+} ions [see Fig. 2]. Note that the helicity-dependent and helicity-independent THz waves change their polarizations by 90° in the temperature interval ~50–70 K (see also the Supplemental Material [29], Fig. S4), which corresponds to the spin reorientation as was determined from the behavior of the spin resonances of the Fe^{3+} sublattices [28]. For example, in the y-cut sample the helicity-dependent emission below 50 K has an electric field polarized along the x axis [Fig. 5(a), open circles], while above 70 K it is along the z axis [Fig. 5(b), open circles].

These facts show that the observed THz emission arises from the light-induced coherence within the $^4I_{15/2}$ ground state of the Er^{3+} ions. The emission disappears above 150 K when the population of the lowest sublevels within the ground state equalizes. Based on the frequencies of the observed modes we attribute them to various transitions between the states belonging to the different Kramers doublets as shown in Fig. 2. The polarizations of the observed components allow us to assign them to the modes of different symmetry in accordance with Table I. The transitions within the doublets have frequencies below the cutoff frequency of our THz spectrometer (~100 GHz) [30] and are not resolved here.

The helicity-dependent THz emission is only observed in the y-cut $ErFeO_3$ sample. Below the spin reorientation temperature interval the helicity-sensitive emitted THz electric field is parallel to the x axis, while above the spin reorientation it is polarized along the z axis [open circles in Figs. 5(a) and 5(b)]. The emission comprises three spectral bands at ~1.3, ~1.5, and ~1.8 THz in the Γ_2 phase, while in the Γ_4 phase only two bands at ~1.5 and ~1.8 THz are observed. The absence of the 1.3 THz band shows that the Raman susceptibility that determines the helicity-dependent excitation is very small for this mode in the
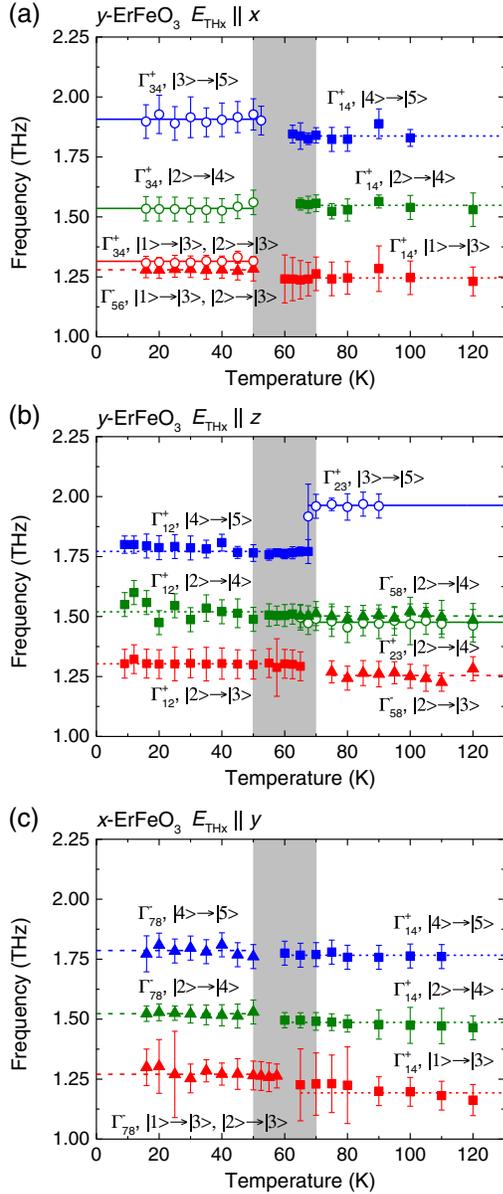
FIG. 5. (a) The central frequencies of the spectral bands are shown vs temperature for the x-polarized emission from the y-cut ErFeO$_3$ sample. (b) The same for the z-polarized emission from the y-cut sample. (c) The same for the y-polarized emission from the x-cut sample. In all panels, the filled symbols correspond to magnetic-dipole (squares) and electric-dipole (triangles) excited modes, which are not sensitive to the pump polarization. The open circles correspond to magnetic-dipole modes excited by the circularly polarized light. The gray area indicates the spin-reorientation temperature interval. The frequencies are assigned to the modes of Er^{3+} ions based on their symmetry.

Γ_4 phase in the y-cut sample. The modes are excited by the circularly polarized pump light propagating along the y axis of the sample, which acts as an effective field along this direction. The symmetry dictates that the m_y magnetic dipole Γ_{23}^+ and Γ_{34}^+ modes are excited below and above the spin-reorientation temperature interval, respectively.

Polarization-independent THz emission has components polarized along both the x and z axes above and below the spin reorientation temperature interval in the y-cut sample. Again, there are three bands centered at $\sim$1.3, $\sim$1.5, and $\sim$1.8 THz. However the frequencies of these components are slightly, but noticeably shifted with respect to the helicity-dependent bands. The polarization-independent emission can be divided into the main component polarized along the z axis in the Γ_2 phase and along the x axis in the Γ_4 phase [squares in Figs. 5(a) and 5(b)] and a smaller orthogonal component most pronounced for the $\sim$1.3 THz band [triangles in Figs. 5(a) and 5(b)]. Therefore, at each $\sim$1.3, $\sim$1.5, and $\sim$1.8 THz frequency, the pump laser pulse excites three oscillating sources of THz emission. Again, the polarization of these components rotates by 90° in the (xz) plane within the spin-reorientation temperature interval. The polarization-independent emission must be assigned not only to the longitudinal-like electric dipole Γ_{56}^- and Γ_{58}^- modes, but also to the magnetic dipole Γ_{12}^+ and Γ_{14}^+ modes. Indeed, the polarization-independent mechanism of ultra-fast excitation of the magnetic-dipole longitudinal-like magnetic modes of Fe^{3+} ions has been recently demonstrated in orthoferrites [25,28].

In the x-cut sample the THz emission is independent of the pump polarization and consists of three spectral bands centered at $\sim$1.3, $\sim$1.5, and $\sim$1.8 THz shown in Fig. 5(c). However, the frequencies of the bands below the spin-reorientation temperature interval are slightly shifted compared to those above this interval. Therefore, we suggest that the emission in the x-cut sample arises from the Γ_{78}^- electric dipole excitations in the low temperature Γ_2 phase. In the high temperature Γ_4 phase the emission arises from the Γ_{14}^+ magnetic dipole modes.

The absence of the helicity-dependent emission in the x-cut sample suggests that the Γ_{23}^+ modes are highly elliptical with $m_y \gg m_x$. Indeed, the precessional mode of the iron sublattices in the orthoferrites is strongly elliptical [31]. The Er magnetic moments are coupled to the Fe spins and, consequently, this coupling favors the high ellipticity of the rare-earth magnetic precession.

In summary, we have demonstrated the possibility of selective ultrafast excitation of magnetic dipole and electric dipole-active modes of the rare-earth ions in ErFeO$_3$ crystals via ISRS. By varying the polarization of light and its propagation direction with respect to the crystallographic axes we have addressed different dipole components of the $4f^{11}$ transitions in the Er^{3+} ions. Importantly, in the case when not only the electric dipole transitions (mostly in the iron sublattices), but also magnetic dipole transitions (mostly in the rare-earth sublattices) contribute to the optical dielectric function, the magnetic dipole-active THz modes respond preferentially to the electric dipole virtual optical transitions, whereas the electric dipole-active THz modes respond mostly to the magnetic dipole virtual optical transitions. Thus, our observations call for

theoretical models beyond the conventional electric dipole approximation. We anticipate the demonstrated ultrafast ISRS is applicable to other rare-earth oxides, as practically in all of them the low-energy states are present. Finally, we note that the magnetic order throughout a broad class of magnetic oxides containing both $3d$ and $4f$ ions can be manipulated by controlling the rare-earth states [32]. Therefore, by femtosecond pumping of rare-earth ions one could exploit coupling between the rare-earth and $3d$ spins like in ErMnO$_3$ [33], DyFeO$_3$ [34], and PrFe$_3$(BO$_3$)$_4$ [35] for revealing new, non-thermal pathways towards ultrafast spin control.

---

*R.Mikhaylovskiy@science.ru.nl

[1] A. Kirilyuk, A. V. Kimel, and Th. Rasing, Ultrafast optical manipulation of magnetic order, Rev. Mod. Phys. **82**, 2731 (2010).

[2] S. L. Johnson *et al.* Femtosecond dynamics of the collinear-to-spiral antiferromagnetic phase transition in CuO, Phys. Rev. Lett. **108**, 037203 (2012).

[3] Y. M. Sheu, S. A. Trugman, L. Yan, Q. X. Jia, A. J. Taylor, and R. P. Prasankumar, Using ultrashort optical pulses to couple ferroelectric and ferromagnetic order in an oxide heterostructure, Nat. Commun. **5**, 5832 (2014).

[4] P. Němec, E. Rozkotová, N. Tesařová, F. Trojánek, E. De Ranieri, K. Olejník, J. Zemen, V. Novák, M. Cukr, P. Malý, and T. Jungwirth, Experimental observation of the optical spin transfer torque, Nat. Phys. **8**, 411 (2012).

[5] T. Kampfrath *et al.*, Terahertz spin current pulses controlled by magnetic heterostructures, Nat. Nanotechnol. **8**, 256 (2013).

[6] T. J. Huisman *et al.*, Femtosecond control of electric currents in metallic ferromagnetic heterostructures, Nat. Nanotechnol. **11**, 455 (2016).

[7] T. Satoh, Y. Terui, R. Moriya, B. A. Ivanov, K. Ando, E. Saitoh, T. Shimura, and K. Kuroda, Directional control of spin-wave emission by spatially shaped light, Nat. Photonics **6**, 662 (2012).

[8] Y. Au, M. Dvornik, T. Davison, E. Ahmad, P. S. Keatley, A. Vansteenkiste, B. Van Waeyenberge, and V. V. Kruglyak, Direct excitation of propagating spin waves by focused ultrashort optical pulses, Phys. Rev. Lett. **110**, 097201 (2013).

[9] A. V. Kimel, A. Kirilyuk, P. A. Usachev, R. V. Pisarev, A. M. Balbashov, and Th. Rasing, Ultrafast non-thermal control of magnetization by instantaneous photomagnetic pulses, Nature (London) **435**, 655 (2005).

[10] T. Satoh, R. Iida, T. Higuchi, M. Fiebig, and T. Shimura, Writing and reading of an arbitrary optical polarization state in an antiferromagnet, Nat. Photonics **9**, 25 (2015).

[11] A. V. Kimel, A. Kirilyuk, A. Tsvetkov, R. V. Pisarev, and Th. Rasing, Laser-induced ultrafast spin reorientation in the antiferromagnet TmFeO$_3$, Nature (London) **429**, 850 (2004).

[12] A. V. Kimel, C. D. Stanciu, P. A. Usachev, R. V. Pisarev, V. N. Gridnev, A. Kirilyuk, and Th. Rasing, Optical excitation of antiferromagnetic resonance in TmFeO$_3$, Phys. Rev. B **74**, 060403R (2006).

[13] A. V. Kimel, B. A. Ivanov, R. V. Pisarev, P. A. Usachev, A. Kirilyuk, and Th. Rasing, Inertia-driven spin switching in antiferromagnets, Nat. Phys. **5**, 727 (2009).

[14] R. Iida, T. Satoh, T. Shimura, K. Kuroda, B. A. Ivanov, Y. Tokunaga, and Y. Tokura, Spectral dependence of photo-induced spin precession in DyFeO$_3$, Phys. Rev. B **84**, 064402 (2011).

[15] J. A. de Jong, A. V. Kimel, R. V. Pisarev, A. Kirilyuk, and T. Rasing, Laser-induced ultrafast spin dynamics in ErFeO$_3$, Phys. Rev. B **84**, 104421 (2011).

[16] J. A. de Jong, I. Razdolski, A. M. Kalashnikova, R. V. Pisarev, A. M. Balbashov, A. Kirilyuk, Th. Rasing, and A. V. Kimel, Coherent control of the route of an ultrafast magnetic phase transition via low-amplitude spin precession, Phys. Rev. Lett. **108**, 157601 (2012).

[17] L. Le Guyader, A. Kleibert, F. Nolting, L. Joly, P. M. Derlet, R. V. Pisarev, A. Kirilyuk, Th. Rasing, and A. V. Kimel, Dynamics of laser-induced spin reorientation in Co/SmFeO$_3$ heterostructure, Phys. Rev. B **87**, 054437 (2013).

[18] D. L. Wood, L. M. Holmes, and J. P. Remeika, Exchange fields and optical Zeeman effect in ErFeO$_3$, Phys. Rev. **185**, 689 (1969).

[19] R. M. White, Review of recent work on the magnetic and spectroscopic properties of the rare-earth orthoferrites, J. Appl. Phys. **40**, 1061 (1969).

[20] A. M. Balbashov *et al.*, Observation in TmFeO$_3$ of direct electronic transitions inside the principal multiplet of a rare-earth ion, JETP Lett. **42**, 564 (1985).

[21] C.-Y. Kuo *et al.*, $k = 0$ Magnetic Structure and Absence of Ferroelectricity in SmFeO$_3$, Phys. Rev. Lett. **113**, 217203 (2014).

[22] A. P. Malozemoff, The optical spectrum and magnetic properties of TmFeO$_3$ in the single-ion model, J. Phys. Chem. Solids **32**, 1669 (1971).

[23] A. M. Balbashov, G. V. Kozlov, S. P. Lebedev, A. A. Mukhin, A. Yu. Pronin, and A. S. Prokhorov, Anomalies of high-frequency magnetic properties and new orientational transitions in HoFeO$_3$, Sov. Phys. JETP **68**, 629 (1989).

[24] A. A. Mukhin and A. C. Prokhorov, Magnetic spectroscopy of antiferromagnetic dielectrics. Rare-earth orthoferrites, Proc. General Physics Institute **25**, 162 (1990). In Russian.

[25] R. V. Mikhaylovskiy, E. Hendry, A. Secchi, J. H. Mentink, M. Eckstein, A. Wu, R. V. Pisarev, V. V. Kruglyak, M. I. Katsnelson, Th. Rasing, and A. V. Kimel, Ultrafast optical modification of exchange interactions in iron oxides, Nat. Commun. **6**, 8190 (2015).

[26] G. Gallot and Grischkowsky, Electro-optic detection of terahertz radiation, J. Opt. Soc. Am. B **16**, 1204 (1999).

[27] D. L. Wood, J. P. Remeika, and E. D. Kolb, Optical spectra of rare-earth orthoferrites, J. Appl. Phys. **41**, 5315 (1970).

[28] R. V. Mikhaylovskiy, E. Hendry, V. V. Kruglyak, R. V. Pisarev, T. Rasing, and A. V. Kimel, Terahertz emission spectroscopy of laser-induced spin dynamics in $TmFeO_3$ and $ErFeO_3$ orthoferrites, Phys. Rev. B **90**, 184405 (2014).

[29] See Supplemental Material at http://link.aps.org/supplemental/10.1103/PhysRevLett.118.017205 for the corresponding temperature dependencies of the amplitudes.

[30] T. J. Huisman, R. V. Mikhaylovskiy, A. Tsukamoto, Th. Rasing, and A. V. Kimel, Simultaneous measurements of terahertz emission and magneto-optical Kerr effect for resolving ultrafast laser-induced demagnetization dynamics, Phys. Rev. B **92**, 104419 (2015).

[31] G. F. Herrmann, Magnetic resonances and susceptibility in orthoferrites, Phys. Rev. **133**, A1334 (1964).

[32] S. Baierl, M. Hohenleutner, T. Kampfrath, A. K. Zvezdin, A. V. Kimel, R. Huber, and R. V. Mikhaylovskiy, Nonlinear spin control by terahertz-driven anisotropy fields, Nat. Photonics **10**, 715 (2016).

[33] L. Chaix et al., Magneto- to electroactive transmutation of spin waves in $ErMnO_3$, Phys. Rev. Lett. **112**, 137201 (2014).

[34] T. N. Stanislavchuk, Y. Wang, Y. Janssen, G. L. Carr, S.-W. Cheong, and A. A. Sirenko, Magnon and electromagnon excitations in multiferroic $DyFeO_3$, Phys. Rev. B **93**, 094403 (2016).

[35] K. N. Boldyrev, T. N. Stanislavchuk, A. A. Sirenko, L. N. Bezmaternykh, and M. N. Popova, Coupling between phonon and crystal-field excitations in multiferroic $PrFe_3(BO_3)_4$, Phys. Rev. B **90**, 121101(R) (2014).